Catalysis Today 158 (2010) 521–529

Contents lists available at ScienceDirect

Catalysis Today

journal homepage: www.elsevier.com/locate/cattod

NiW/AMBT catalysts for the production of ultra-low sulfur diesel

Guofu Wan[a,b], Aijun Duan[a,*], Ying Zhang[c], Zhen Zhao[a,*], Guiyuan Jiang[a], Dengqian Zhang[a], Jian Liu[a], Keng Chung[d]

[a] State Key Laboratory of Heavy Oil Processing, China University of Petroleum, Beijing 102249, PR China
[b] College of Mechanical and Energy Engineering, Jiangsu Polytechnic University, Changzhou 213016, PR China
[c] Department of Materials Science and Engineering, University of Petroleum, Beijing 102249, PR China
[d] Department of Chemical and Petroleum Engineering, University of Calgary, Calgary, T2N 1N4 Canada

ARTICLE INFO

Keywords:
Hydrodesulfurization
Tungsten and nickel catalyst
Ultra-low sulfur diesel
Titania
Zeolite

ABSTRACT

A series of hydrodesulfurization (HDS) catalysts of NiW supported on γ-Al_2O_3–MB–TiO_2 (denoted as AMBT) composites with various amounts of TiO_2 were prepared, in which zeolite MB was synthesized from kaolin mineral. The samples were characterized by means of N_2 physisorption, XRD, UV–vis DRS, TPR, NH_3-TPD, XPS, HRTEM and NO-DRIFT. The characterization results showed that, compared with NiW/Al_2O_3, the additions of MB and TiO_2 reduced the interaction between the metal components and the composite support, and also made the active metal phase of WS_2 existing as larger slabs on the surface of the composite support. Meanwhile, the layer number of the active metal clusters became greater. Furthermore, the incorporation of MB into the support tuned the overall acidity of the NiW catalysts. The active metal species of W and Ni exhibited higher sulfidation extents in NiW/AMBT catalyst than those in NiW/Al_2O_3 and NiW/AMB catalysts. The HDS activities of FCC diesel changed with the addition amounts of TiO_2 in the NiW/AMBT catalysts. Higher HDS efficiencies were achieved over NiW/AMBT5 and NiW/AMBT9 than that of traditional NiW/Al_2O_3 catalyst, and the optimal TiO_2 content was 9 m% in the AMBT composite supports. The reason of NiW/AMBT catalyst with higher HDS activity was attributed to the enhanced hydrogenation activity. The ultra deep desulfurization of FCC diesel oil, in which the sulfur content was below 10 ppm, could be obtained under the operation conditions of 350 °C, 5 MPa, 1 h^{-1} and 600 mL/mL.

1. Introduction

As one of the most important technology the hydrotreating process can improve the diesel quality apparently. Increasingly stringent environmental regulations in the sulfur content of diesel fuel have created an urgent need for highly hydrodesulfurization (HDS) catalysts [1,2]. In the future, so called ultra-low sulfur diesel (below 15 ppm S) should be required to meet the environmental regulation and fuel specifications [3]. It has been reported that the strict specification of ultra clean diesel requires a relatively higher catalytic activity of HDS which might be four or five times greater than that of the traditional catalysts [4]. As a result, several approaches have been applied to achieve an excellent HDS catalyst, especially the development of new materials is an important choice for achieving suitable support candidate in the catalyst design.

One of the important factors that affect the efficiency of a HDS catalyst is the interaction between the active phases and the support. Support–metal interactions (SMI) influence not only on the dispersion of the active components, but also on their reducibility and sulfidability, e.g., modification of the morphology of the sulfided active phase, interaction of chemical environment of acid sites. Some results have been summarized in reviews and open literatures concerning hydrotreatment catalyst and deep HDS [5–8]. Since cobalt or nickel molybdenum/tungsten sulfides have been established as the active species for the desulfurization, the better support to promote their activity and selectivity in the reaction steps of HDS has been paid much attention, while γ-alumina support has been widely used in the commercial catalysts because of their excellent mechanical as well as dispersing properties against sulfides. Support plays an important role in determining the nature and the number of active sites, and consequently affects the catalytic activity of catalyst. In the past two decades, a lot of intense activities in the world have been made on the development of different mixed oxide supports which favored the enhancement of the activity of Mo-based or W-based HDS catalysts. Recently, TiO_2-supported molybdenum/tungsten catalysts have attracted more interests [9] by means of their higher reducibility to a lower valence state of molybdenum/tungsten and their higher catalytic activity for HDS compared with alumina-supported materials. Neverthe-

* Corresponding author. Tel.: +86 10 89731586; fax: +86 10 69724721.
E-mail addresses: duanaijun@cup.edu.cn (A. Duan), zhenzhao@cup.edu.cn (Z. Zhao).

0920-5861/$ – see front matter © 2010 Elsevier B.V. All rights reserved.
doi:10.1016/j.cattod.2010.08.021

less, the low specific surface area and limited thermal stability of TiO_2-support inhibit its wide use in the commercial processes. To overcome the above disadvantages the mixed oxides of titania with alumina have been adopted as supports to take advantage of the favorable characteristics of both systems [10]. TiO_2–Al_2O_3 oxide-supported Mo- or W-based catalysts have been successfully used for the hydrodesulfurization of refractory molecules such as 4,6-DMDBT or fuel feeds and Ti-containing catalysts should be good candidates for hydrogenation of aromatics and deep HDS of diesel fuels [11]. Recently, it was reported that mixed supports containing zeolites and alumina exhibited high activities in DBT HDS process due to the addition of acidic zeolites into the catalyst components, and zeolite Y was most widely used in HDS catalysts [12,13]. It is believed that the addition of acidic components in HDS catalysts can improve the hydroisomerization and dealkylation activities, and thus 4,6-DMDBT, known to be a representative molecule for "hard-to-desulfurize", can be effectively converted into sulfur-free products due to the elimination effect of the steric hindrance by acidic components in the HDS catalyst [14,15]. Recently, research works on the application of acidic zeolite β in diesel HDS have also been reported [13,16].

The main objective of this study is to investigate the HDS performances of the supported NiW catalysts of which the supports were the composite carrier of alumina, zeolite MB (zeolite β prepared from kaolin mineral) and titania, and the titania-containing catalysts with various titania contents. In this work, a series of Al_2O_3–MB (denoted as AMB) and $TiO_2(x)$–Al_2O_3–MB (denoted as AMBT) composites-supported NiW catalysts were prepared and their catalytic performances for deep HDS of diesel were evaluated. It was found that the NiW/AMBT9 catalyst gave the highest catalytic activity for the deep HDS of diesel.

2. Experimental

2.1. Preparation of AMBT composite supports

MB zeolite was prepared by in-situ crystallization method from kaolin according to our previous work [17]. The protonated form of MB zeolite (denoted as H-MB) was obtained by calcined NH_4-MB at 500 °C for 5 h. The preparation route of Al_2O_3–MB–$TiO_2(x)$ has been described in elsewhere. H-MB powder was dispersed uniformly in deionized water, the obtained suspension was added dropwise into the pseudoboehmite sol. Subsequently, a part of the sol mixture was transferred and stirred vigorously in a water bath at 75 °C until the mixture became a viscous paste; and titanium-sol (made from the tetra-n-butyl-titanate, ethanol, nitric acid and deionized distilled water with the molar ratio of 1:15:0.3:3) was dripped into another part of sol under the drastic stirring condition to form the gel and further stirred vigorously in a water bath at 75 °C until the mixture became viscous paste. Then the obtained gels were dried at 120 °C for 4 h, calcinated at 550 °C for 4 h. The obtained supports were designed as AMBT*x*, the weight ratio of Al_2O_3 and H-MB was kept as 2.1:1 in all AMBT*x* supports, where *x* is denoted as TiO_2 weight ratio in the AMBT*x* supports. These supports were ready for metal impregnation.

2.2. Preparation of supported NiW catalysts

The supported NiW catalysts were prepared by using co-impregnation and incipient-wetness impregnation method with an aqueous solution of the appropriate amounts of ammonium metatungstate hydrate [$(NH_4)_6W_{12}O_{39}{\cdot}H_2O$] and nickel nitrate hexahydrate [$Ni(NO_3)_2{\cdot}6H_2O$]. After impregnation, the catalyst precursors were dispersed in an ultra-sonic unit for 30 min. Then the prepared samples were dried at 110 °C for 12 h, and calcined at 500 °C for 4 h. All the catalysts were prepared with the constant loadings of W and Ni (corresponding to 27 m% of WO_3 and 3.5 m% of NiO, respectively).

2.3. Catalyst characterization

Porosity and surface area measurements of samples were performed on a Micromeritics ASAP 2020 automated gas adsorption system. All the samples were outgassed at 350 °C under vacuum prior to N_2 adsorption at −196 °C. Mercury porosimetry experiments were carried out on a Micromeritics AutoPore IV 9500 apparatus in the pressure range 0–30,000 psia. The UV–vis diffuse reflectance spectra (DRS) experiments were performed on a Hitachi U-4100 UV–vis spectrophotometer with the integration sphere diffuse reflectance attachment. The powder samples were loaded in a transparent quartz cell and were measured in the region from 200 to 800 nm under ambient conditions using $BaSO_4$ standard reflectance as the baseline for the catalyst measurement. X-ray powder diffraction (XRD) profiles were recorded in an XRD-6000 diffractometer using Cu Kα radiation under 40 kV, 30 mA, scan range from 5° to 80° at a rate of 4° min^{-1}. Afterwards, H_2-TPR was carried out using 10% hydrogen in argon at a constant flow rate of 40 mL min^{-1}, from room temperature to 1000 °C, at a heating rate of 10 °C min^{-1}. The acidic property of the catalyst was determined by temperature-programmed desorption of ammonia (NH_3-TPD). The experiments were carried out in the range of 120–600 °C in a fix-bed flow microreactor. The molecules desorption from sample were monitored on-line by a TCD. Prior to the NH_3-TPD experiments, sample (200 mg) was outgassed at 500 °C for 1 h in a flow of dry helium (30 mL min^{-1}). Subsequently, sample was cooled down to 120 °C and saturated for about 30 min in a flow of NH_3 (40 mL min^{-1}). Then, sample was purged in a helium flow until a constant baseline level was attained. Desorption was carried out with a linear heating rate (10 °C min^{-1}) in a flow of He (40 mL min^{-1}). HRTEM measurements of the sulfided catalysts were carried out on a Tecnai G2 F20 transmission electron microscope (Philips) operated at an accelerating voltage of 200 kV. The catalysts were sulfided with a 2 m% CS_2/cyclohexane mixture at 320 °C for 6 h and placed in cyclohexane before measurement. The XPS spectra of the samples were taken on an ESCA Lab 220i-XL electron spectrometer (VG) using 300 W Mg Kα radiation. The binding energies were corrected by using the C1 s peak at 284.6 eV as reference. The characterization of diffuse reflectance infrared Fourier transform (DRIFT) measurements used NO as a probe molecule to study the distribution of coordinatively unsaturated sites (CUS). The catalysts were sulfided with a 2 m% CS_2/cyclohexane mixture at 320 °C for 6 h, and were loaded in the IR shell and flashed He at 150 °C for 30 min, then cooled to room temperature. 5% NO/He mixture flew over the sample for 30 min to reach the balance of NO adsorption, subsequently turned to He flow for 30 min. FT-IR spectra of NO were collected at room temperature using FTS-3000 spectrophotometer manufactured by American Digilab company.

2.4. HDS activity measurement

HDS performance was evaluated in a high-pressure fixed-bed reactor with 2 g of catalyst (grain sizes of 0.3–0.5 mm). All the catalysts were presulfided for 6 h with a 2 m% CS_2-cyclohexane mixture under the conditions of LHSV (Liquid Hoursly Space Velocity) of 1.0 h^{-1}, temperature of 320 °C, total pressure of 4 MPa and a H_2/cyclohexane ratio of 600 mL mL^{-1}. HDS tests of diesel were carried out under the conditions of 350 °C, 5.0 MPa, 600 mL·mL^{-1} and 1.0 h^{-1}. Catalytic activities were measured at steady states after 13 h on-stream.

Table 1
Specific surface areas, pore volumes and pore diameters of NiW/AMBT catalysts.

Samples	TiO_2/m%	S_{BET}/$m^2\ g^{-1}$	V_{BJH}/$cm^3\ g^{-1}$	Average pore diameter/nm
NiW/AMB	0	194.10	0.22	3.70
NiW/AMBT2	2	171.73	0.20	3.61
NiW/AMBT5	5	172.77	0.22	3.78
NiW/AMBT9	9	174.37	0.23	3.83
NiW/AMBT14	14	172.40	0.22	3.67
NiW/AMBT24	24	164.83	0.21	3.78

The total sulfur content in the feed and products was measured by using a LC-4 coulometric sulfur analyzer system. The distributions of sulfur species in feed and products were identified by Finnigan Trace GC/MS with a Trace Ultral gas chromatograph using a HP-5MS ($30 \times 0.25 \times 0.25$) capillary column and a pulsed flame photometric detector (PFPD). The catalytic activity under investigation was estimated by the HDS efficiency.

3. Results and discussion

3.1. Catalyst characterization

3.1.1. N_2 adsorption

The textural properties and pore size distributions of catalysts are typically shown in Table 1. Compared with NiW/AMB catalyst, the specific surface areas of NiW/AMBT catalysts decrease after the TiO_2 is introduced to the NiW/AMB catalyst due to the low surface area of TiO_2, while there is no apparent changes when TiO_2 weight content is below 14%, and when TiO_2 weight content is as higher as 24%, the specific surface areas of NiW/AMBT catalysts decrease sharply. However, the addition of TiO_2 only has a slight effect on the pore volumes and average pore diameters.

3.1.2. XRD

Fig. 1 presents the XRD patterns of NiW/AMBT series catalysts. The characteristic diffraction peaks of γ-Al_2O_3 appear in all the spectra of oxide catalysts, either do the characteristic diffraction peaks of MB. With the increasing of TiO_2 contents, the diffraction peak intensities of MB and γ-Al_2O_3 decrease. No XRD diffraction peaks assigned to crystallines of NiO or $NiAl_2O_4$ are found in the oxide catalysts. In fact, for NiW/AMBT14 and NiW/AMBT24 catalysts with higher TiO_2 contents, the characteristic peaks corresponding to WO_3 are observed by XRD. The existence of bulk WO_3 means a lower dispersion degree of active metals and will decrease the hydrodesulfurization activity of the catalysts, which is affirmed by the hydrodesulfurization results. XRD analysis also shows the presence of anatase TiO_2 on NiW/AMBT catalysts.

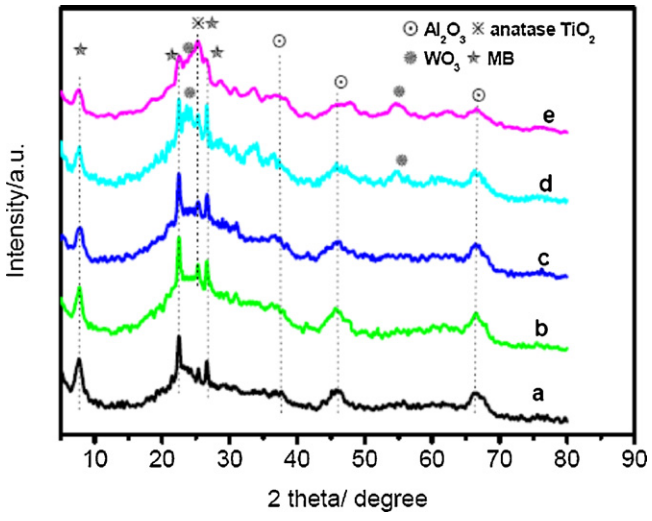

Fig. 1. XRD patterns of NiW/AMBT catalysts: (a) NiW/AMB; (b) NiW/AMBT5; (c) NiW/AMBT9; (d) NiW/AMBT14; (e) NiW/AMBT24.

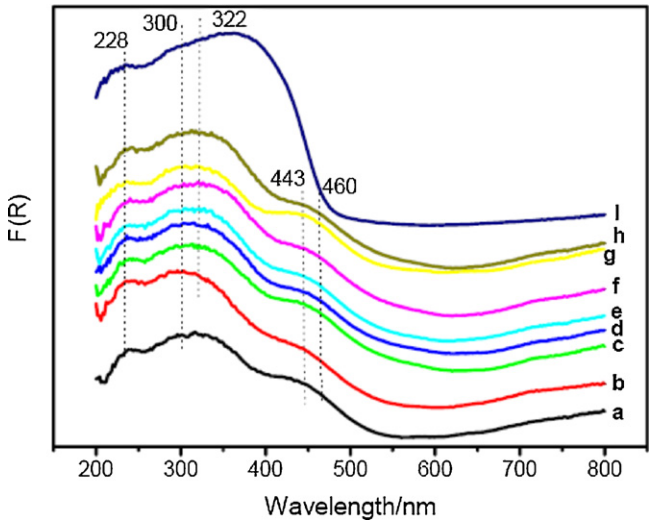

Fig. 2. The UV–vis DR spectra of different catalysts. (a) NiW/Al_2O_3; (b) NiW/AMB; (c) NiW/AMBT0.5; (d) NiW/AMBT2; (e) NiW/AMBT5; (f) NiW/AMBT9; (g) NiW/AMBT14.

3.1.3. UV–vis DRS

The UV–vis DR spectra was applied to determine the structures of supported NiW catalysts in the 200–800 nm region. In Fig. 2, it can be noted that, compared with NiW/Al_2O_3, the NiW/AMBT series catalysts show broad absorption bands from 230 to 320 nm [18,19]. The band at about 260–340 nm is ascribed to the ligand–metal charge transfer: $O^{2-} \rightarrow W^{6+}$ in W–O–W bridge-bonds in polymeric structures [18,19]. The band around 230–280 nm is attributed to tetrahedron or octahedron tungstenic species. The band around 280–340 nm is assigned to tungstic oxide and octahedron tungstenic species which make it more easy for the formation of coordinatively unsaturated species or sulfur vacancies and thus it is in favor of HDS reaction [18,19]. From Fig. 2, comparing the peak intensities around 300 nm with each others, which are attributed to the octahedron tungstenic species, one can find that NiW/AMBT catalysts show higher relative intensities than those of NiW/Al_2O_3 and NiW/AMB catalysts. The differences between the peak intensities imply that the NiW/AMBT catalysts form more octahedron tungstenic species than NiW/Al_2O_3 and NiW/AMB, suggesting that the NiW/AMBT catalysts may be easier to form type II active phase of WS_2 with higher HDS activity after sulfidation, since octahedron tungstenic species are the precursors of type II WS_2. And it can be inferred that NiW/AMBT catalysts maybe show higher hydrogenation activity.

Another characteristic absorption band in the UV–vis spectra of the catalysts is the broad band in the region from 440 to 800 nm region, which is due to d–d transitions of octahedrally coordinated Ni^{2+} [20,21]. With the increase of TiO_2 content in the catalyst, the intensities of the bands around 440 nm increase and shift to high wavelength, indicating an enhanced incorporation of nickel with tungsten to produce Ni–W–O species [22–24], which are the precursors of Ni–W–S phase.

The changes in the positions and intensities of the bands in the spectra of the supported NiW oxide catalyst may be due to the differences of the strength of interaction between nickel, tungsten species and the supports.

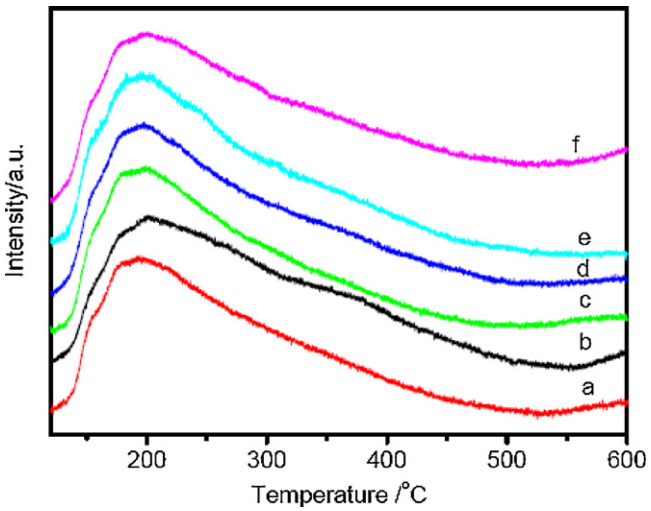

Fig. 3. NH_3-TPD profiles of different catalysts. (a) NiW/Al_2O_3; (b)NiW/AMB; (c) NiW/AMBT5; (d) NiW/AMBT9; (e) NiW/AMBT14; (f) NiW/AMBT24.

3.1.4. NH_3-TPD

NH_3-TPD of the supported NiW oxide catalysts are shown in Fig. 3. It is observed that the shapes of the corresponding desorption curves are parallel, suggesting similar distributions of acidic sites over NiW/Al_2O_3, NiW/AMB and NiW/AMBT series catalysts. The analysis results of NH_3-TPD confirm that those supported NiW catalysts, of which the AMBT composite supports containing TiO_2 and MB were used as supports have large amounts of weak acid (around 110 °C) and small amounts of middle strong acid (around 300 °C) sites, which would facilitate the HDS reactions and avoiding over-cracking of diesel oil.

3.1.5. H_2-TPR

The H_2-TPR profiles of the supported NiW oxide catalysts are shown in Fig. 4. The TPR profiles of all the supported NiW oxide catalysts show two principal reduction peaks in the temperature ranges of 600–800 °C, and 800–1000 °C, respectively. The broad peak at high temperature can be assigned to the superimposed reduction of tetrahedrally coordinated tungsten species and nickel species and the low temperature peak can be ascribed to the reduction of polymeric octahedral tungsten species [25–27]. Moreover, compared with NiW/Al_2O_3 and NiW/AMB catalysts, the locations of

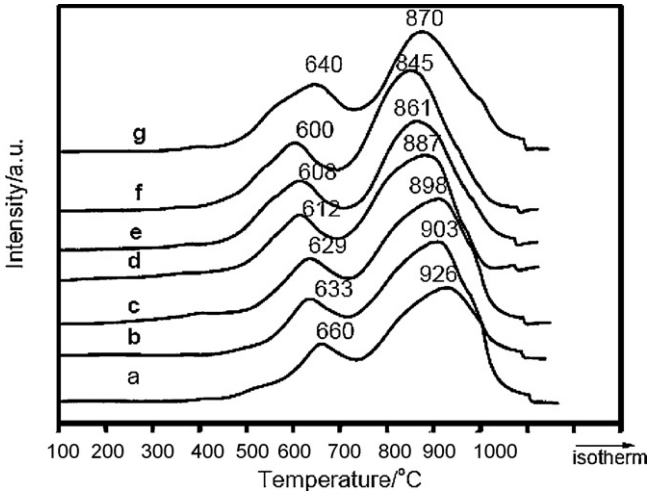

Fig. 4. H_2-TPR profiles of different catalysts. (a) NiW/Al_2O_3; (b)NiW/AMB; (c) NiW/AMBT2; (d) NiW/AMBT5; (e) NiW/AMBT9; (f) NiW/AMBT14; (g) NiW/AMBT24.

Table 2
XPS results of the sulfided catalysts.

Catalysts	$W^{+4}{}_{sul}/W_{total}$	Ni_{sul}/Ni_{total}
NiW/Al_2O_3	0.42	0.58
NiW/AMB	0.50	0.62
NiW/AMBT5	0.53	0.71
NiW/AMBT9	0.69	0.70
NiW/AMBT14	0.62	0.66
NiW/AMBT24	0.64	0.68

two intense peaks of NiW/AMBT catalysts shift toward lower temperatures with the increase of TiO_2 contents, implying that metal oxide species over the NiW/AMBT catalysts have weaker interaction with the AMBT supports than that over Al_2O_3 or AMB supports. It is known that the strong interaction between W species and supports leads to the formation of more stable type of W^{4+} species. The less polarized bonds of polytungstates are more easily reduced than those of the species directly bonded to support. Therefore, the addition of TiO_2 has tuned the metal–support interactions, which causes easier reduction of nickel and tungsten species.

3.1.6. XPS

X-ray photoelectron spectroscopy has been used in order to obtain valuable information about the electronic nature of nickel and tungsten surface species on the state of sulfide phase. As for the curve fitting profiles of the XPS spectra in Fig. 5, a doublet peak appears at 34.4 and 32.5 eV, which are the typical characteristics of tungsten sulfide (WS_2) [28]. In the Ni 2p3/2 spectra (Fig. 6), the peak at 853.8 eV is assigned to nickel sulfide species, and that of 856.6 eV is attributed to nickel oxide species [29–31]. The bands at ca. 862 eV are satellite peaks. The degree of sulfidation of W or Ni species is determinded from the curve fitting, based on the equation of $M_{sulfide}/M_{total} = W_{sulfide}/(M_{oxide} + M_{sulfide})$, M = W or Ni. The results (see Table 2) show that the sulfidation degrees of W species and Ni species in both NiW/AMB and NiW/AMBT catalysts are much higher than that of NiW/Al_2O_3, which may be due to the difference in the interactions of metal species with the support in different catalysts. High sulfidation degree may lead to higher HDS activity [32,33].

3.1.7. HRTEM

The representative HRTEM images of the sulfided NiW catalysts are shown in Fig. 7. The dark WS_2 crystallites fringes are visualized in the HRTEM images. Multi-layered WS_2 slabs are mostly observed in NiW/AMB and NiW/AMBT series catalysts unlike the one-layer slabs exhibited in NiW/Al_2O_3 catalyst.

Based on statistical analysis results in 15 images including about 280 slabs which were taken from the different areas of each catalyst, average lengths and stacking numbers of the WS_2 slabs over the supported NiW catalysts are presented in Table 3. Compared those results of NiW/Al_2O_3 and NiW/AMB with those of NiW/AMBT series catalysts, the longer WS_2 slab lengths and higher WS_2 layer numbers are found in the latters. It is probably related to the different textures of the supports, due to the addition of MB and TiO_2. High WS_2 stacking degree in sulfided catalysts will lead to the formation of type II WS_2 phase [33,34], which possesses higher hydrogenation activity than type I WS_2 phase.

3.1.8. NO-DRIFT

The surface structure of sulfided NiW catalysts are characterized by means of diffuse reflectance infrared Fourier transform (DRIFT) measurements using NO as a probe molecule to study the distribution of coordinatively unsaturated sites (CUS). The DRIFT spectra of NO adsorbed on sulfided NiW catalysts are shown in Fig. 8. The 1710 and 1785 cm^{-1} bands are attributed to the contributions of NO absorbed on WS_2, and the band at 1840 cm^{-1} is the charac-

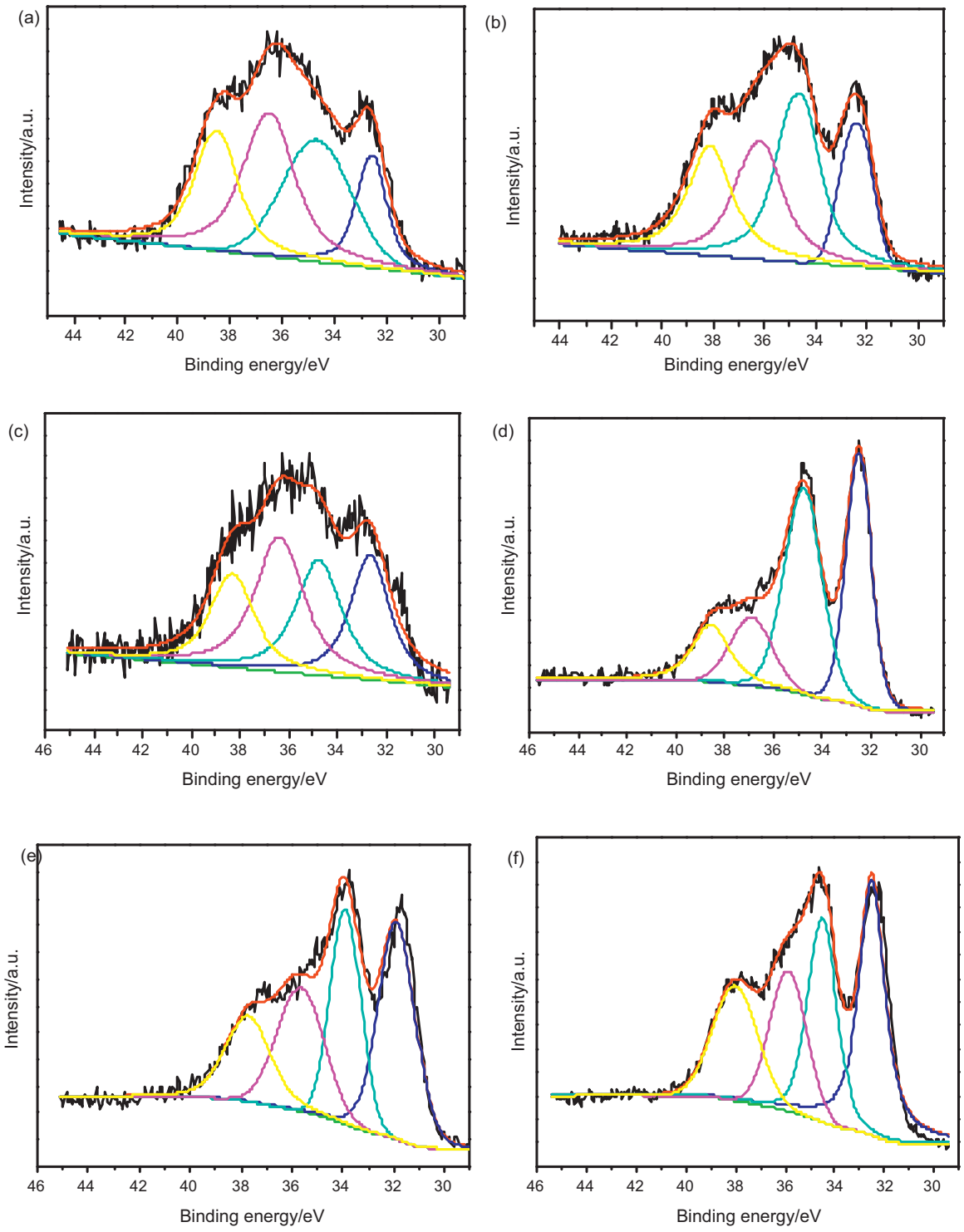

Fig. 5. W4f XPS spectra of the sulfided catalysts with different amounts of titanium. (a) NiW/Al_2O_3; (b) NiW/AMB; (c) NiW/AMBT5; (d) NiW/AMBT9; (e) NiW/AMBT14; (f) NiW/AMBT24.

Table 3
Average slab length and stacking number of WS2 in the sulfided catalysts with different amounts of titanium.

	NiW/Al_2O_3	NiW/AMB	NiW/AMBT5	NiW/AMBT9	NiW/AMBT14	NiW/AMBT24
L/nm	4.1	9.4	9.0	8.9	9.5	9.7
N	1.8	3.1	2.7	2.4	2.8	3.0

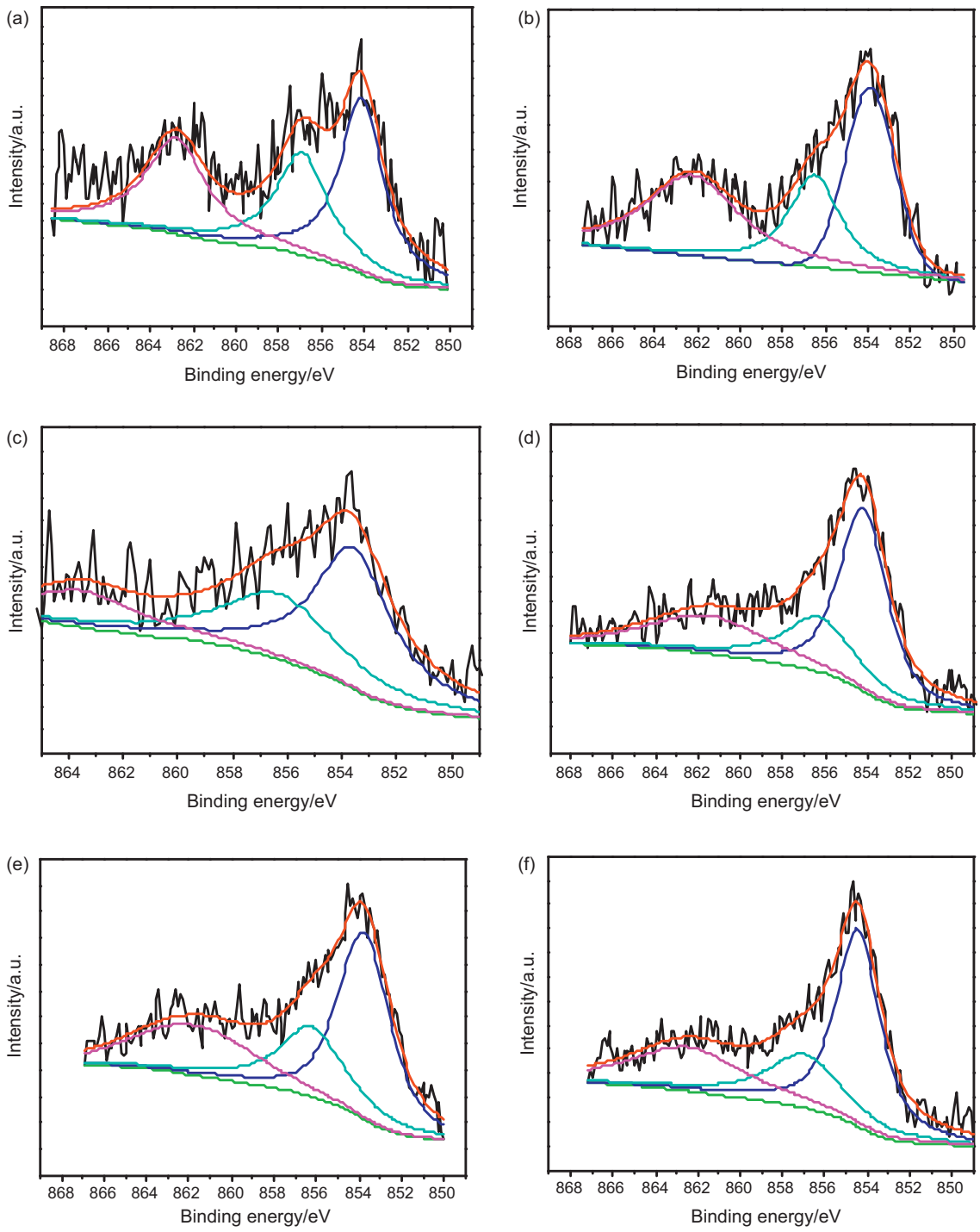

Fig. 6. Ni2p XPS spectra of the sulfided catalysts with different amounts of titanium. (a) NiW/Al_2O_3; (b) NiW/AMB; (c) NiW/AMBT5; (d) NiW/AMBT9; (e) NiW/AMBT14; (f) NiW/AMBT24.

teristic of NO adsorbed on sulfide Ni^{2+} species [35,36]. It can be seen that the intensities of the bands at 1710 cm^{-1} for NiW/AMBT5 and NiW/AMBT9 catalysts are relatively higher than those of the other catalysts. These observations imply that NiW/AMBT5 and NiW/AMBT9 catalysts maybe possess more CUS, which can achieve high HDS activity.

3.2. Catalytic activity

The diesel HDS results are exhibited in Fig. 9 and Table 4. Compared with NiW/Al_2O_3, its HDS efficiency equals to 97.5%, the HDS activities of NiW/AMB, NiW/AMBT5 and NiW/AMBT9 series catalysts increase by 1.2%, 1.8% and 2.2%, respectively. So the optimal TiO_2 content is 9 m% in the composite AMBT supports, and the sulfur content is below 10 ppm obtained under the operation conditions of 350 °C, 5 MPa, 1 h^{-1} and 600 mL/mL, which can meet the Euro V fuel specification of ultra clean diesel.

From Table 4, the sulfur distributions imply that alkyl-substituted DBT compounds are mainly retained compounds in the products. NiW/AMBT5 and NiW/AMBT9 exhibit higher HDS conversions of alkyl-substituted DBT than NiW/Al_2O_3, it is obvious that the addition of suitable amounts of MB and TiO_2 to the catalyst sup-

port leads to higher HDS catalytic activities than the conventional alumina-supported counterpart.

The increase in HDS activity of NiW/AMBT catalysts is likely due to the synergy effect, which seems to be related to the mutual interaction of metal species, Al_2O_3, MB and TiO_2.

It can be infered that the addition of acidic MB zeolite in NiW/AMBT catalysts improve the hydroisomerization and dealkylation activities, and the refractory sulfur compounds such as 4,6-DMDBT can be effectively converted into sulfur-free products due to the reduction of steric hindrance through the dealkylation and transalkylation [14,15]. And the appropriate amount of zeolite added in the AMBT catalyst will not cause over-cracking according to the analysis results of NH_3-TPD.

The additions of MB and TiO_2 reduce the interaction between the metal components and the support, and tune the redox properties and/or sulfidation abilities of the catalysts, as can be seen from the characterization results of TPR and XPS. The sulfidation extents of tungsten increase in NiW/AMBT series catalysts, which could be beneficial to improve the HDS activities [32,33].

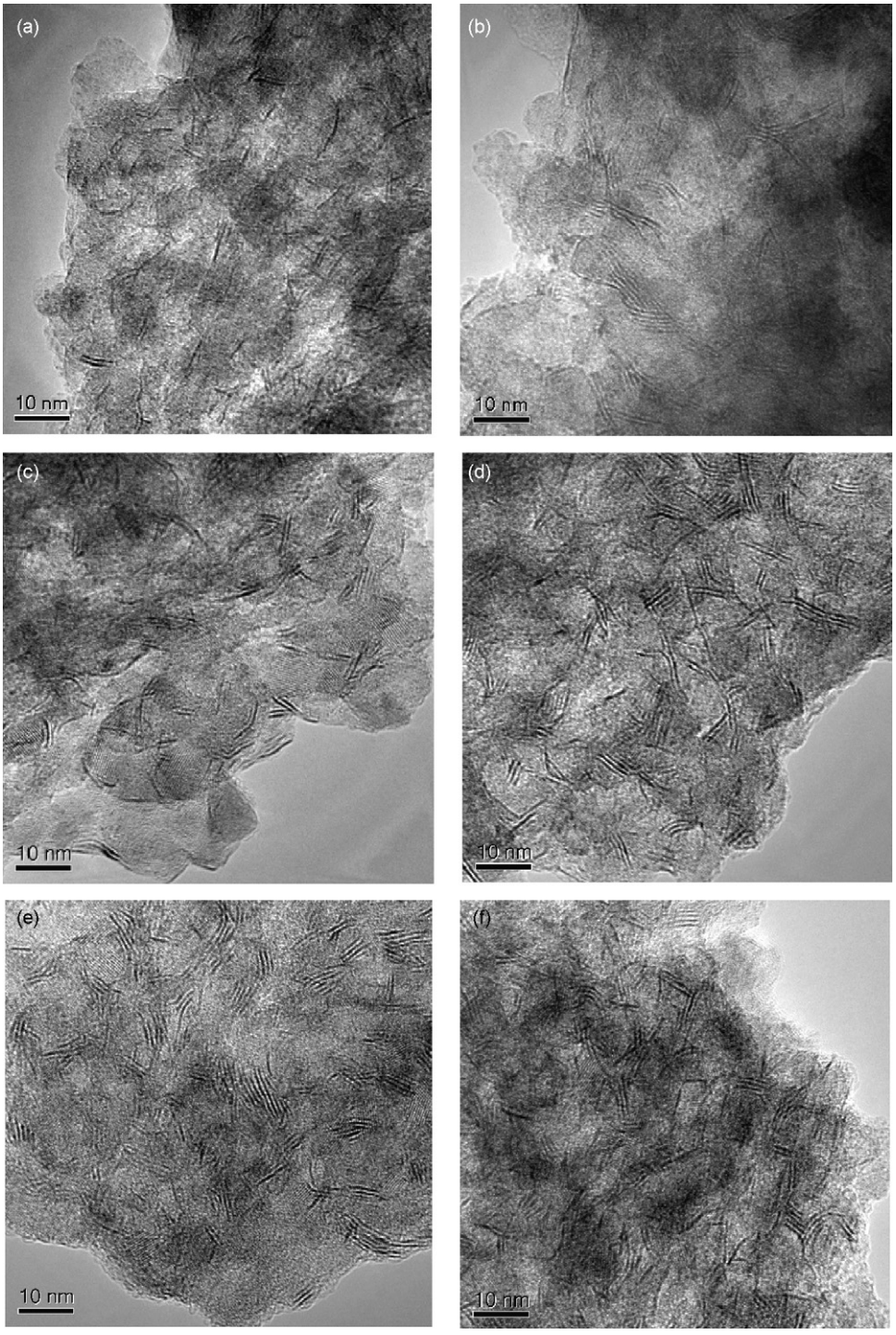

Fig. 7. The HRTEM images of the sulfided catalysts with different amounts of titanium. (a) NiW/Al_2O_3; (b) NiW/AMB; (c) NiW/AMBT5; (d) NiW/AMBT9; (e) NiW/AMBT14; (f) NiW/AMBT24.

Table 4
The sulfur compounds in feed and in products after HDS over NiW/Al_2O_3, NiW/AMB, NiW/AMBT9 catalysts.

Sulfur compound	Feed/μg g^{-1}	NiW/Al_2O_3/μg g^{-1}	NiW/AMB/μg g^{-1}	NiW/AMBT9/μg g^{-1}
BT	28.8	–	–	–
C1-BT	145.2	–	–	–
C2-BT	249.5	–	–	–
≧C3-BT	345.2	–	–	–
DBT	53.8	–	–	–
C1-DBT	135.1	–	–	–
C2-DBT	146.2	11.8	8.0	2.7
≧C3-DBT	196.3	20.4	8.7	1.2
Total	1300	32.2	16.7	3.9

From HRTEM results, NiW/AMBT catalysts show much higher WS_2 slab sizes and layers than those of NiW/Al_2O_3. It is believed that multi-layered WS_2 slabs may provide a higher density of CUS and more edge sites compared with single-layered slabs, and thus the high stacking numbers of WS_2 slabs can enhance the HYD activity [37].

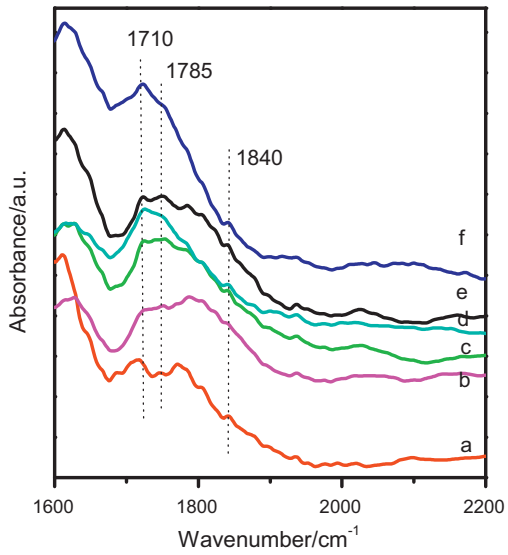

Fig. 8. DRIFT spectra of NO adsorbed on the sulfided catalysts with different amounts of titanium. (a) NiW/Al_2O_3; (b) NiW/AMB; (c) NiW/AMBT5; (d) NiW/AMBT9; (e) NiW/AMBT14; (f) NiW/AMBT24.

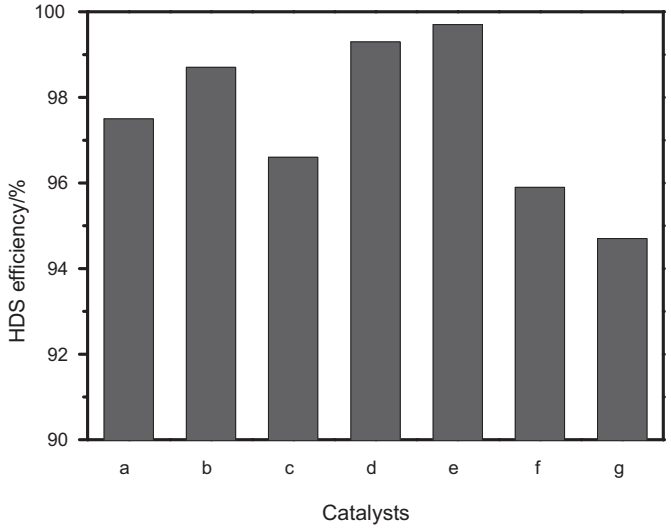

Fig. 9. HDS efficiencies of FCC diesel over the sulfided catalysts with different amounts of titanium. (a) NiW/Al_2O_3; (b) NiW/AMB; (c) NiW/AMBT1; (d) NiW/AMBT5; (e) NiW/AMBT9; (f) NiW/AMBT14; (g) NiW/AMBT24.

After the addition of MB and TiO_2 to Al_2O_3 support, the sulfidation degree of W species and the WS_2 slab sizes increase significantly, which facilitate the hydrogenation performance of NiW/AMBT catalysts. It seems that there exist a compromise between WS_2 slab sizes and stacking degree for achieving optimal catalyst performance. Moreover, the increase in hydrogenation performance of the NiW/AMBT5 and NiW/AMBT9 catalysts could be derived from the electronic promotion effect of TiO_2. The titania acted as promoters of the W phase give rise to a synergy effect, which seems to be related to the electronic properties of the partially reduced and/or sulfided TiO_2 surface and, in particular, to the presence of Ti^{3+} ions [38,39]. Ti^{3+} maybe the "electronic promoters" for the active W sulfide phases and more easily favors the formation of CUS or sulfur vacancies, as a result, the HDS activity could be greatly promoted [40].

4. Conclusions

The additions of MB zeolite and TiO_2 tune the interaction between W species and the support, and improve the sulfidation extent of active metals. The incorporation of acidic zeolite and/or electronic promoter into the composite support leads to a longer lengths and a higher stacking numbers of the WS_2 slabs, which facilitates the formation of more active type II sites with higher hydrogenation reactivity. NiW/AMBT9 catalyst shows the highest HDS efficiency of 99.7%, and the sulfur content in product can meet the Euro V fuel specification of ultra clean diesel.

Acknowledgments

The authors acknowledge the financial supports from Natural Science Foundation of China (no. 20876173, no. 20833011 and no. 20773163), Ministry of Education key project of China (no. 31) and CNPC-Petrochemical Research Institute project (No. 2008A-3801).

References

[1] D.D. Whitehurst, H. Farag, T. Nagamatsu, Catal. Today 45 (1998) 299.
[2] J.J. Lee, H. Kim, S.H. Moon, Appl. Catal. B 41 (2003) 171.
[3] N. Kunisada, K.H. Choi, Y. Korai, I. Mochida, K. Nakano, Appl. Catal. A: Gen. 273 (2004) 287.
[4] K. Knudsen, B. Cooper, H. Topsoe, Appl. Catal. A: Gen. 189 (1999) 205.
[5] H. Topsøe, B.S. Clausen, F.E. Massoth, in: J.R. Anderson, M. Boudart (Eds.), Hydrotreating Catalysts Catalysis Science and Technology, vol. 11, Springer, Berlin, 1996.
[6] P.T. Vasudevan, J.L.G. Fierro, Catal. Rev. Sci. Eng. 38 (1996) 161.
[7] D.D. Withehurst, T. Isoda, I. Mochida, Adv. Catal. 42 (1998) 345.
[8] C. Song, Catal. Today 86 (2003) 211.
[9] Z.B. Wei, W. Yan, H. Zhang, T. Ren, Q. Xin, Z. Li, Appl. Catal. A: Gen. 167 (1998) 39.
[10] G. Murali, B. Srinivas, M. Kumar, S. Maity, Catal. Today 86 (2003) 45.
[11] W. Huang, A. Duan, Z. Zhao, G. Wan, G. Jiang, T. Dou, K.H. Chung, J. Liu, Catal. Today 131 (2008) 314.
[12] D. Solís, A. López Agudo, J. Ramírez, T. Klimova, Catal. Today 116 (2006) 469.
[13] L. Ding, Y. Zheng, Z. Zhang, Z. Ring, J. Chen, J. Catal 241 (2006) 435.

[14] G. Pérot, Catal. Today 86 (2003) 111.
[15] N. Kunisada, K. Choi, Y. Korai, I. Mochida, K. Nakano, Appl. Catal. A: Gen. 276 (2004) 51.
[16] G. Wan, A. Duan, Y. Zhang, Z. Zhao, G. Jiang, D. Zhang, Z. Gao, J. Liu, K.H. Chung, Energy and Fuels 23 (2009) 3846.
[17] G. Wan, A. Duan, Y. Zhang, Z. Zhao, D. Zhang, Z. Gao, G. Jiang, Prep. Pap. -Am. Chem. Soc., Div. Pet. Chem. 53 (2008) 203.
[18] A.A. Gutiérrez, J. Ramírez, G. Busca, Catal. Lett. 56 (1998) 29.
[19] A.A. Gutiérrez, J. Ramírez, G. Busca, Langmuir 14 (1998) 630.
[20] S. Damyanova, A. Spojakina, K. Jiratova, Appl. Catal. A: Gen. 125 (1995) 257.
[21] A. Spojakina, P.L. Damyanova, Appl. Catal. 56 (1989) 163.
[22] C.J. Song, C. Kwak, S.H. Moon, Catal. Today 74 (2002) 193.
[23] P. Atanasova, T. Tabakova, Ch. Vladov, T. Halachev, A. Lopez Agudo, Appl. Catal. A: Gen. 161 (1997) 105.
[24] P. Atanasova, T. Halachev, Appl. Catal. A: Gen. 108 (1994) 123.
[25] B. Scheffer, P. Molhoek, J.A. Moulijn, Appl. Catal. 46 (1989) 11.
[26] C. Dirk, C. Pieter, J. Catal. 116 (1989) 309.
[27] L. Karakonstantis, H. Matralis, Ch. Kordulis, A. Lycourghiotis, J. Catal. 162 (1996) 306.
[28] S. Bendezú, R. Cid, J.L.G. Fierro, A. López Agudo, Appl. Catal. A: Gen. 197 (2000) 47.
[29] M. Sun, T. Burgi, R. Cattaneo, R. Prins, J. Catal. 197 (2001) 172.
[30] H. Topsøe, B. Hinnemann, J.K. Nørskov, J.V. Lauritsen, F. Besenbacher, P.L. Hansen, G. Hytoft, R.G. Egeberg, K.G. Knudsen, Catal. Today 107–108 (2005) 12.
[31] M. Sun, T. Burgi, R. Cattaneo, D. van Langeveld, R. Prins, J. Catal. 201 (2001) 258.
[32] E.J.M. Hensen, P.J. Kooyman, Y. van der Meer, et al., J. Catal. 199 (2001) 224.
[33] E.J.M. Hensen, V.H.J. de Beer, J.A.R. van Veen, et al., Catal. Lett. 84 (2002) 59.
[34] M. Breysse, P. Afanasiev, C. Geantet, et al., Catal Today 86 (2003) 5.
[35] T. Halachev, P. Atanasova, A. Lopez Agudo, et al., Appl. Catal. A: Gen. 136 (1996) 161.
[36] H.R. Reinhoudt, E. Crezee, A.D. van Langeveld, et al., J. Catal. 196 (2000) 315.
[37] L. Vradman, M.V. Landau, M. Herskowitz, Fuel 82 (2003) 633.
[38] J. Ramirez, L. Ceden, G. Busca, J. Catal. 184 (1999) 59.
[39] G.D. Panagiotou, T. Petsi, K. Bourikas, C. Kordulis, A. Lycourghiotis, J. Catal. 262 (2009) 266.
[40] G. Liu, J.A. Rodriguez, J. Hrbek, B.T. Long, D.A. Chen, J. Mol. Catal. A: Chem. 202 (2003) 215.